CSM: Contact Sensitivity Maps for Benchmarking Robot Collision Handling Systems

Robin Jeanne Kirschner, João Jantalia, Nico Mansfeld, Saeed Abdolshah and Sami Haddadin

Abstract— In physical human-robot interaction (pHRI), robots need to detect and react to intended and unintended contacts in a safe manner. Proprioceptive sensing capabilities and collision detection and identification techniques differ among commercially available robots, which means that also their sensitivity to detect dynamic collisions with the environment or the human co-worker differ. Up to now, there exists no standardized procedure for assessing the contact sensitivity of a robotic system. In this paper, we propose the concept of contact sensitivity maps (CSM), a relationship between the robot's dynamic impact properties and the reliability of its collision handling. The CSM allows the robot user to determine for which robot workspace areas and dynamic collision parameters (mass, velocity) reliable contact detection and reaction can be expected. We propose a standardized benchmarking procedure and test setup for deriving CSMs. Finally, we analyze and compare the experimental results of the Universal Robots UR10e, UR5e, and Franka Emika Panda, where we observe significant differences in contact sensitivity.

I. INTRODUCTION

Lightweight collaborative robots are nowadays widely used in industrial and domestic applications. Benchmark tests are highly important for designing and selecting the most appropriate system for certain tasks. Besides classical performance metrics like repeatability, reachability, and payload capacity, also the inherent robot safety characteristics are important design criteria for collaborative robots [1], [2]. This includes the probability of human injury during contact [3], [4] and the collision sensing and handling capabilities [5]. Many collision detection and reaction schemes have been proposed and are listed in [6]. They rely on different proprioceptive robot measurements, e.g., motor current or joint torque. The sensing capabilities and the selected collision detection and identification technique largely influence the robot's contact sensitivity, i.e., the ability to detect and react to even small external forces. However, to the best of the authors' knowledge, so far no standardized metrics or experimental protocols have been proposed to assess and quantify a robot's contact sensitivity.

In this paper, we propose a standardized benchmark for object contact sensitivity (CS) in dynamic scenarios. Inspired by the work in [3] we propose the concept of a so-called contact sensitivity map (CSM) that relates the robot's CS to the object mass and robot velocity involved in the collision. The CSM allows the robot user to determine for which robot
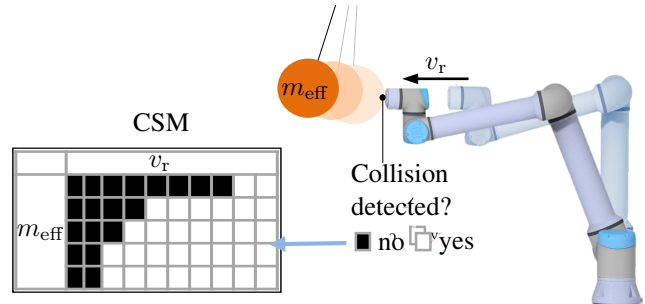
All authors are with Institute for Robotics and Systems Intelligence, Munich School of Robotics and Machine Intelligence, Technical University of Munich, 80797 Munich, Germany robin-jeanne.kirschner@tum.de

Fig. 1. Experimental evaluation of the robot contact sensitivity in dynamic contact situations. The robot velocity is denoted v_r whereas the effective mass of the obstacle in the robot motion direction is given by m_{eff}.

workspace areas and dynamic collision parameters (mass, velocity) the collision detection is reliable. This information is crucial for task planning and ensuring human safety during task execution, e.g., in hand-over tasks. To derive the CSMs, we design a pendulum test setup (see Fig. 1) and propose a standardized test protocol that can be applied to any serial robot manipulator. The benchmark experiments are carried out for three robots, namely the Universal Robots UR5e and UR10e and the Franka Emika Panda. Here, we

- evaluate and compare the CSM of the three robots,
- analyse the influence of force and torque thresholds as well as different contact detection methods, and
- evaluate the influence of the robot configuration/pose on the CSM.

This paper is structured as follows. Section II gives a brief overview of collision handling and existing collision benchmarks. In Sec. III, we define the CSM and introduce a standardizable procedure to generate CSMs. In Sec. IV we describe the considered collision dynamics, the pendulum test device, and the three established experiments. In Sec. V we present the results for all experiments. Finally, Sec. VI concludes the paper.

II. STATE OF THE ART

Robotic collision handling in pHRI consists of five different phases, which form the so-called collision handling pipeline [6]:

1. detection,
2. isolation,
3. identification,
4. classification and
5. reaction.

The five collision handling phases can be implemented using different sensing strategies, e.g. collision detection schemes

Preparation

Increment mass,
Increment velocity, j++

Repeat ≥ 3 times   if $R < 1$ or $j = m$ if $R = 1$

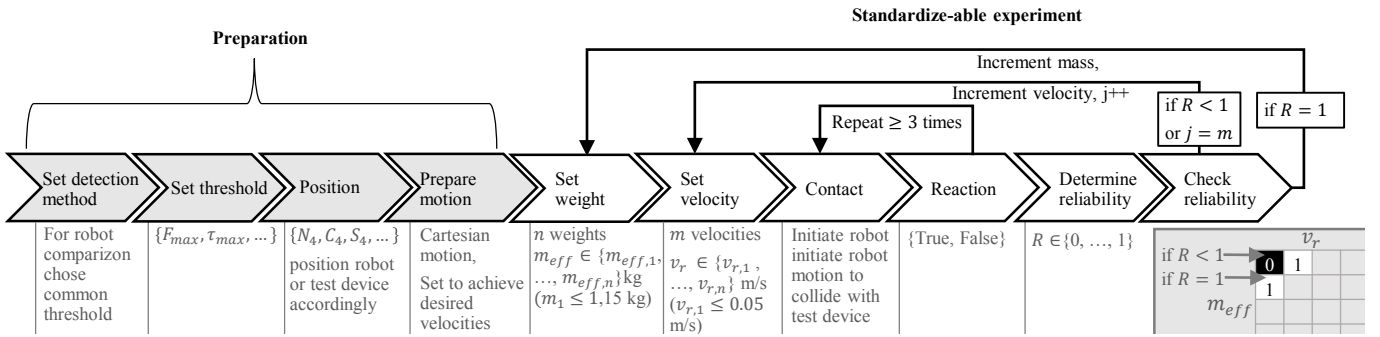| Set detection method	Set threshold	Position	Prepare motion	Set weight	Set velocity	Contact	Reaction	Determine reliability	Check reliability
For robot comparizon chose common threshold	$\{F_{max}, \tau_{max}, ...\}$	$\{N_4, C_4, S_4, ...\}$ position robot or test device accordingly	Cartesian motion, Set to achieve desired velocities	n weights $m_{eff} \in \{m_{eff,1}, ..., m_{eff,n}\}$ kg $(m_1 \leq 1{,}15$ kg$)$	m velocities $v_r \in \{v_{r,1}, ..., v_{r,n}\}$ m/s $(v_{r,1} \leq 0.05$ m/s$)$	Initiate robot initiate robot motion to collide with test device	$\{$True, False$\}$	$R \in \{0, ..., 1\}$	if $R < 1$; if $R = 1$ v_r, m_{eff}

Fig. 2. Standardized testing procedure for the derivation of a CSM.

using momentum observers [7] or motor torque disturbance observers [8]. Further developments on collision handling schemes were adapted using additional sensing systems e.g. Kinect cameras [9] or robot learning approaches [10], [11]. Even though multiple contact detection strategies exist, no standardized procedure to evaluate contact sensitivity is known to the authors. To obtain the robot motion sensitivity, the authors in [12] propose the use of sensitivity functions based on the dynamic and kinematic parameters of the robot, such as the angle and distance between the links and the robot mass matrix. Such models allow integration into the robot control, but require full knowledge of the robot inertial parameters and can become computationally expensive [12]. For contact sensitivity such a sensitivity model increases in complexity as additional contact parameters need to be considered.

For comparing collision handling systems experimental analysis was proposed in [6]. In [13], a benchmark for collision detection algorithms is introduced, which compares the time required by the robot to make a decision and perform braking in different scenarios. Besides braking time also contact force is a possible benchmark, which can be measured using commonly available devices such as in [5]. Constrained contact force maps are proposed in [14] as a benchmark for the severity of harm resulting from a collision in constrained contact scenarios.

Other robot benchmarks focus on e.g. the user-experience during motion planning [15] or on task-dependent metrics such as listed in [16]. To benchmark robot perception, authors use the success rate of recognition as benchmark [16], which can be adapted to obtain a CS benchmark. Standardized benchmarks for motion performance of industrial robots, such as repeatability and accuracy, are listed in the ISO 9283:1998 standard [17]. For performance analysis, the standard defines reference positions for each robot system based on their minimum and maximum reach. These reference cubes enable reproducible measurements for different robots and are thus relevant for any kind of benchmark.

III. DEFINITION CONTACT SENSITIVITY MAP (CSM) AND EXPERIMENTAL PROTOCOL

We define the term contact sensitivity (CS) as the robot's capability to recognize and react to an external contact. The process of contact recognition requires the detection, isolation, and identification of the contact, which depends on the robot's sensing capabilities, the collision detection scheme, and the selected collision threshold among other parameters. In this paper, we are concerned with the end user's point of view, i.e., the collision detection schemes, parameterization options, and interfaces are considered that are provided by the manufacturer. Based on the idea of describing the success rate of a contact detection and the reference cube provided by ISO 9283:1998, we propose a new benchmark for CS focusing on unconstrained contacts.

In practice, robots may collide with objects of different size/weight and at varying speeds. In this paper, we consider blunt unconstrained collisions, the object is initially at rest. In terms of contact sensitivity, it is important for the user to know whether the robot can detect both a fast collision with a heavy object and a rather slow collision with a light object. Let the mass range of the object be $m_{\text{eff}} \in [m_{\text{eff,min}}, m_{\text{eff,max}}]$ and the robot velocity range $v_{\text{r}} \in [v_{\text{r,min}}, v_{\text{r,max}}]$. We want to determine the contact sensitivity for each (discretized) pair $(m_{\text{eff}}, v_{\text{r}}) \,|\, m_{\text{eff}} \in [m_{\text{eff,min}}, m_{\text{eff,max}}], v_{\text{r}} \in [v_{\text{r,min}}, v_{\text{r,max}}]$ involved in a collision, i.e., whether the collision can be detected reliably or not. We define the mapping of the mass and velocity pair to contact sensitivity as the contact sensitivity map (CSM), which is illustrated in Fig. 1. The reliability of contact detection is denoted by $R \in [0, 1]$, where $R < 1$ is considered as unreliable and $R = 1$ as reliable. If $R = 1$, we enter a 1 (white area) in the CSM, otherwise 0 (black area). Besides the object mass and robot velocity, the CSM mainly depends on

- the **robot configuration**, which can be specified using the joint configuration q or according to the reference cube described in ISO 9283 [17], which allows comparing different robots (see Sec. IV),
- the **robot collision detection** scheme that can be selected by the user, and
- **collision thresholds** that can be selected by the user within a certain range.

To generate the CSM for the selected collision detection parameters and robot configuration, we propose the procedure illustrated in Fig. 2. In the preparation phase, the robot configuration, collision detection scheme, and thresholds are selected. In the experiment the robot collides

with an initially resting, unconstrained object that has the mass m_{eff}, which can be adjusted in the discretized range $m_{\text{eff}} \in [m_{\text{eff,min}}, m_{\text{eff,max}}]$. For the discretized robot velocities $v_{\text{r}} \in [v_{\text{r,min}}, v_{\text{r,max}}]$ (starting with the lowest velocity) the contact detection reliability is determined by repeating the collision at least three times[1]. The success or failure occurrence of a collision detection/reaction is noted after every impact to evaluate R. As depicted in Fig. 2 (bottom right), the reliability of the contact detection ($R = 1$ or $R < 1$) is then assigned to the CSM. If $R = 1$ then we increment the mass, if $R < 1$ then we increment velocity. The procedure is repeated until all considered object masses and robot velocities are tested. The chosen object mass for the following experiments covers the range of the suggested effective mass for safety critical body parts such as head ($4.4 kg$) or neck ($1.2 kg$) according to ISO/TS 15066:2016 [1]. The robot velocity is oriented on the safe velocity of $250 mm/s$ stated in ISO/DIS 10218-2:2020 [18]. of special interest is the detection of collisions occurring at unsafe velocities, which harbour a hazard potential for human co-workers. Nevertheless, a tactile robot should reliably detect contact also at velocities below $250 mm/s$. Therefore, also experiments with lower velocity are conducted.

IV. EXPERIMENTAL DESIGN

This section motivates and explains the energy-based benchmark for CS and the design of the experiments using a pendulum setup for CS analysis.

A. Collision Dynamics

We consider a dynamic, unconstrained collision of the robot with an object (or a human body part), which is initially at rest. The scalar effective mass and velocity of the object are denoted by m_{eff} and v_{obj}, the effective mass and velocity of the robot during impact are m_{r} and v_{r}, respectively. The robot quantities can be obtained as follows. The robot link side dynamics[2] can be expressed as

$$M(\boldsymbol{q})\ddot{\boldsymbol{q}} + C(\boldsymbol{q},\dot{\boldsymbol{q}})\dot{\boldsymbol{q}} + g(\boldsymbol{q}) = \boldsymbol{\tau} + \boldsymbol{\tau}_{\text{ext}}, \qquad (1)$$

with $\boldsymbol{q} \in \mathbb{R}^n$ and $\dot{\boldsymbol{q}} \in \mathbb{R}^n$ representing link positions and velocities. The link inertia matrix is denoted by $M(\boldsymbol{q}) \in \mathbb{R}^{n \times n}$, the Coriolis matrix by $C(\boldsymbol{q},\dot{\boldsymbol{q}}) \in \mathbb{R}^{n \times n}$, and the gravity vector by $g(\boldsymbol{q}) \in \mathbb{R}^n$. The joint torque is denoted by $\boldsymbol{\tau} \in \mathbb{R}^n$ and the external torque by $\boldsymbol{\tau}_{\text{ext}} \in \mathbb{R}^n$. The robot mass perceived at the contact location in the Cartesian unit direction of impact $\boldsymbol{u} \in \mathbb{R}^3$ is [19]

$$m_{\text{r}} = \left(\boldsymbol{u}^{\mathsf{T}} \boldsymbol{\Lambda}_{\nu}(\boldsymbol{q})^{-1} \boldsymbol{u} \right)^{-1}, \qquad (2)$$

which is also referred to as the reflected mass. Here, $\boldsymbol{\Lambda}_{\nu}^{-1}(\boldsymbol{q})$ is the upper 3×3 matrix of the robot Cartesian mass matrix inverse

$$\boldsymbol{\Lambda}(\boldsymbol{q})^{-1} = \boldsymbol{J}(\boldsymbol{q})\boldsymbol{M}(\boldsymbol{q})\boldsymbol{J}(\boldsymbol{q})^{\mathsf{T}}, \qquad (3)$$

[1]Three repetitions are used for safety collision measurement to obtain ISO/TS 15066 conformity.
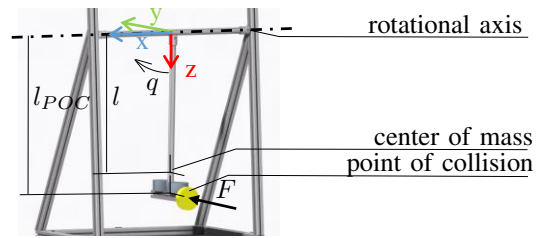
[2]Here, only rigid link/joint robots are considered.

Fig. 3. CAD-model of the pendulum test setup.

where $\boldsymbol{J}(\boldsymbol{q}) \in \mathbb{R}^{n \times m}$ is the Jacobian matrix at the contact location. The Cartesian translational robot velocity in direction $\boldsymbol{u}$ is given by

$$v_{\text{r}} = \boldsymbol{u}^{\mathsf{T}} \boldsymbol{J}_{\nu}(\boldsymbol{q})\dot{\boldsymbol{q}}, \qquad (4)$$

with $\boldsymbol{J}_{\nu}(\boldsymbol{q})$ being the upper $3 \times n$ part of $\boldsymbol{J}(\boldsymbol{q})$. Finally, for the collision we assume conservation of momentum

$$m_{\text{eff}}v_{\text{obj}} = m_{\text{r}}v_{\text{r}}. \qquad (5)$$

B. Pendulum Model

We propose using a pendulum, which allows exchangeable masses, static and dynamic collision and adjustable contact surfaces. The pendulum consists of ball-bearings with low friction and a rod. Attached to the rod is a profile, which allows to mount weights and exchangeable contact geometries or materials of varying stiffness. We use the model depicted in Fig. 3 to obtain the perceived mass $m_{\text{p,eff}}$ at the point of collision (POC) described by l_{POC}.

The generated torque τ around the fixed axis of rotation x-axis at collision is

$$\tau = Fl_{\text{POC}} = J_{xx}\ddot{q}, \qquad (6)$$

with the force F acting on the POC right after collision and the radius of gyration l_{POC}. The moment of inertia J_{xx}, force F and the angular acceleration $\ddot{q}$ can be written as

$$J_{\text{xx}} = J_{\text{xx}}^{(\text{S})} + m_{\text{p}}l^2, \qquad (7)$$

$$F = m_{\text{p,eff}}\ddot{y}, \qquad (8)$$

and

$$\ddot{q} = \frac{\ddot{y}}{l_{\text{POC}}}, \qquad (9)$$

leading to the perceived mass

$$m_{\text{p,eff}} = \frac{J_{xx}^{(\text{S})} + m_{\text{p}}l^2}{l_{\text{POC}}^2}, \qquad (10)$$

at the POC with $l_{\text{POC}} = 780$ mm. We increase the load of the pendulum m_{p} as described in Table I.

We use a collision material simulating the human skin on the thighs with 30 ShA, which is recommended for collision safety measurement based on ISO/TS 15066 [1].

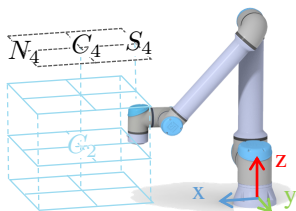| m_p [kg]	$J_{xx}^{(\mathrm{S})}$ [gmm^2]	l [mm]	$m_\mathrm{p,eff}$ [kg]
1.50	107	629	1.15
2.30	120	666	1.87
3.30	128	687	2.77
4.30	135	686	3.55
5.30	140	686	4.33
6.30	149	678	5.00
7.30	156	672	5.67

Fig. 4. ISO 9283:1998 reference cube defined by the center point C_2 and positions C_4, N_4 and S_4.

C. Considered Robot Configurations

To evaluate the CS we refer to the safety braking reaction of the three robotic arms UR10e, UR5e and FE Panda. We use a contact point, where the z-axis of the robot's end-effector is pointing in Cartesian x-direction and the robot moves linearly in x-direction until it recognizes a contact. As we define the contact points based on the reference cube following ISO 9283:1998 for all robots an extension of the reference cube is required. We define this additional horizontal layer as a parallel surface to the other layers, setting the position C_4 to be at twice the height of C_2, as shown in 4. Referring to ISO 9283:1998, the cube size $400mm$ is applied as cube length, l_c for the FE Panda and UR5e. For the UR10e we represent the workspace using the cube length of $800mm$. The linear motion is performed starting from S_4, along the axis to N_4, and ending at the end of the robot's workspace. We define C_4 as point of contact for the first two experiments. All points are defined using ISO 9283:1998 and are listed in Table II.

	Panda	UR10e	UR5e
l_c [mm]	400	800	400
S_4 [mm]	$[298, 0, 652]$	$[326, 0, 981]$	$[236, 0, 563]$
C_4 [mm]	$[498, 0, 652]$	$[726, 0, 981]$	$[436, 0, 563]$
N_4 [mm]	$[698, 0, 652]$	$[1126, 0, 981]$	$[636, 0, 536]$

To exclude the influence of an end-effector, the robot only collides with the flange as shown in Fig. 5. By varying v_r at the contact we increase the energy transferred to the pendulum during contact and expect also reliable contact detection for lower masses using higher velocities.

For generating a CSM using the pendulum testing device we follow the procedure explained in Sec. IV and shown in Fig. 2 and determine different maps using C_4 (experiments
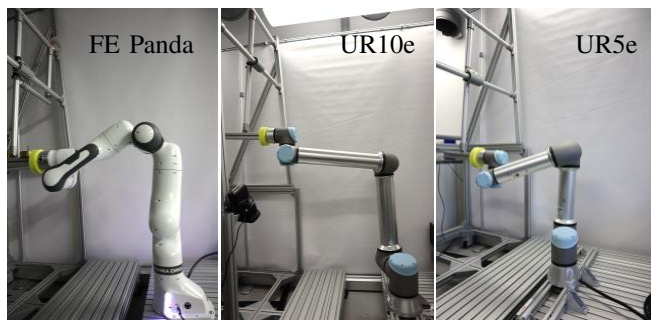

Fig. 5. Pendulum test set up for CS with FE Panda, UR10e, and UR5e at their respective C_4-positions.

1 and 2) and N_4, C_4, S_4 (experiment 3) as collision points. The experiments are explained below. The selected masses are listed in Table I.

The experimental set ups for all robots are shown in Fig. 5.

1) Experiment 1 - 100 N Contact Threshold: The goal of this experiment is to show whether different robot types react to an occurring contact due to their embedded CS, which is considered unknown to the user, i.e. their sensor systems and contact isolation and identification algorithms. For this purpose, we use comparable collision detection strategies for each robot's safety braking function and the same value of the defined threshold. In this case the force thresholds at the robot flange are used. For both UR robots the minimum adjustable tool force is $F_\mathrm{max} = 100N$. Therefore, in this experiment the collision threshold $F_\mathrm{max} = 100N$ is set for all three robots. For the UR robots this requires changing the safety setting to the most sensitive option. To avoid slowing down due to the speed limits, we select the custom safety settings and select $1000mm/s$ as the upper safety threshold for speed. The Panda robot's collision behaviour setting is adjusted using the Franka Control Interface (FCI). Using the FCI, the user can set collision and contact thresholds described by a 6-DoF wrench at the end-effector. To trigger the safety braking, both collision thresholds are set to $[100N, 100N, 100N, 100Nm, 100Nm, 100Nm]$. Additionally, the Pandas interfaces FCI and FE Desk enable the selection of joint torque thresholds. For the joint torque thresholds, we use the maximum values suggested by FE Desk to eliminate their influence on the braking reaction. Finally, we follow the procedure described by Fig. 2 to obtain the CSMs for FE Panda and both UR robots.

2) Experiment 2 - Comparison Force and Torque Thresholds: Some robots allow the user to use different methods for collision detection. Depending on the contact scenario, it is important to know whether the detection method is more or less sensitive. To compare collision detection methods, we generate the CSMs for the most sensitive setting of FE Panda with two different collision detection methods - force/torque thresholds at the end-effector and torque thresholds for all joints. We use a linear trajectory in Cartesian space along the axis from S_4 to C_4 using a fourth-order Cartesian trapezoidal motion profile. The acceleration is set to $1.0m/s^2$. The FCI allows users to set any six-dimensional

vector of positive doubles for the force contact thresholds on the end-effector. Also for the joint torque thresholds any seven-dimensional vector of positive doubles can be set as thresholds. To find the most sensitive thresholds for both contact detection methods, we conduct a small-scale preliminary study to investigate which thresholds could be used to produce repeatable motion. For this, we performed the intended linear motion ten times without the pendulum and observed if any errors occurred. The occurrence of an error that interrupts the movement early leads to the exclusion of the current set of thresholds. We started with thresholds $0.5N$ and $0.5Nm$ for forces and torques and increased them in $0.5N/step$. Through this previous investigation, we found that the lowest force thresholds for repeatable motions are $[10N, 10N, 10Nm, 10Nm, 10Nm]$ for force/torque thresholds at the end-effector. As the most sensitive torque thresholds for all seven joints, we found that $\boldsymbol{\tau}_{\max} = [2.5, 2.5, 1.75, 1.25, 1.25, 1.00, 1.00]Nm$ can be applied[3]. After applying the thresholds accordingly, two CSMs are generated to compare their performance.

D. Experiment 3 - Comparison N_4, C_4, and S_4 Position

The robot pose influences motion sensitivity as stated in [12]. It also influences the effective mass at a contact location and thus the transferred energy during contact.

In this experiment, to find out whether the robot pose also has an effect on the CS, we compare the CS at C_4-position with that at N_4- and S_4-positions. Prior to the experiment, we determine m_r of the FE-Panda robot for each of the above positions by simulation, e.g. (2). We use the Cartesian pose for S_4, C_4, and N_4 with the flange pointing in positive x-direction as depicted by Fig. 6. Then we define the robot configuration with the robot elbow pointing upward by constraining the robot joint motions. By applying the inverse kinematics of the robot 30 times, we obtain 30 joint configurations for which we derive m_r using the dynamic robot model determined by [20]. To estimate the expected robot effective mass that occurs during the experiment we use the average of all 30 masses for each of the three reference positions. As shown in Fig. 6, the average effective mass differs between all three positions on a small scale, so we expect slight variations in the CS of the robot.

For contact at S_4 the robot needs to start its motion at $x = 0.22m$ to avoid singular joint positions. To obtain the CSMs, we apply the most sensitive torque setting applicable with our setup for FE Panda $\boldsymbol{\tau}_{\max} = [2.5, 2.5, 1.75, 1.25, 1.25, 1.00, 1.00]Nm$.

V. RESULTS AND DISCUSSION

In this section, we provide the results for the three experiments described in IV. The CSMs for all investigated robots, contact detection methods, and varying positions are depicted in one comparative CSM each. In addition, approximated CS-curves are shown that allow CS to be compared. The use

[3]Please note that the limitation for the torque and force thresholds here results from the applied motion generator. A motion generator of higher order might enable the use of even lower thresholds.
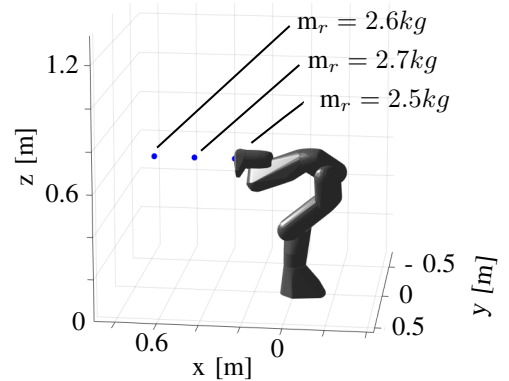

Fig. 6. Robot configuration for simulation of the effective mass at the robot flange at S_4-position and results for the expected m_r during experiments for S_4-, C_4-, and N_4-position.
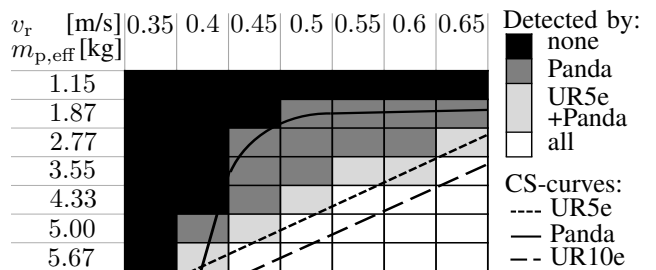

Fig. 7. Comparative CSM for unconstrained contacts using the UR10e, UR5e and Panda robot and setting the applicable contact force/torque threshold $100N/100Nm$ for each robot.

of these curves allows estimating the ability to detect contact with a given object and can be used to obtain data-driven contact sensitivity functions for robot control. The results focus on brief comparisons between CS of the investigated experimental conditions and discuss the applicability of the obtained CSMs for robot integration.

A. Experiment 1

For a robot CS performance analysis using comparable collision detection settings, we show the CS for the FE Panda, UR10e, and UR5e in Fig. 7. While for FE Panda the CS-curve suggests a logarithmic shape, for both UR robots it is rather linear within the measured range of mass and velocity. The Panda robot is therefore able to detect contact in 63% of the displayed cases. The UR5e is capable of detecting the contact in 39% of collisions and the UR10e in 27%. Even using force/torque sensing at the end-effector as a common collision detection method, all three robots show different CS behavior. The higher mass of the UR10e compared to the smaller UR5e appears to be disadvantageous for the CS. Another general conclusion from this experiment is, that there appears to be a great influence of the robot velocity and the effective mass of the object on CS. In a working scenario, considering the CSMs during planning or control helps to understand and estimate which contacts with human coworkers or obstacles can be safely detected and reacted to and which ones will fail.
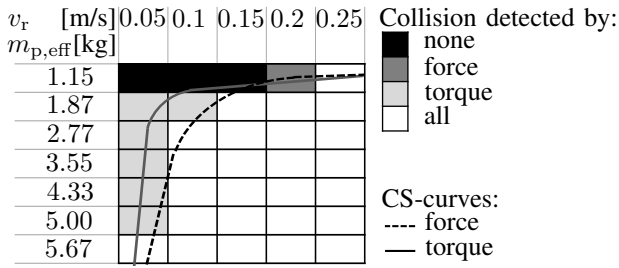
v_r [m/s]	0.05	0.1	0.15	0.2	0.25	Collision detected by:
$m_\mathrm{p,eff}$[kg]						■ none
1.15						▨ force
1.87						▥ torque
2.77						□ all
3.55						
4.33						CS-curves:
5.00						---- force
5.67						— torque

Fig. 8. CSM for unconstrained contacts with the Panda robot using the joint torque thresholds $\boldsymbol{\tau}_\mathrm{max} = [2.5, 2.5, 1.75, 1.25, 1.25, 1.00, 1.00]Nm$ compared to using the measured end-effector force/torque as threshold with $10N/10Nm$.

v_r [m/s]	0.05	0.1	0.15	0.2	0.25	Collision detected at:
$m_\mathrm{p,eff}$[kg]						■ none
1.15						▨ N_4
1.87						▥ N_4+S_4
2.77						□ all
3.55						
4.33						CS-curves:
5.00						---- N_4
5.67						— C_4
						– – S_4

Fig. 9. Comparative CSM for unconstrained contacts at N_4, C_4, and S_4 position with upright elbow using Panda robot with the joint torque thresholds $\boldsymbol{\tau}_\mathrm{max} = [2.5, 2.5, 1.75, 1.25, 1.25, 1.00, 1.00]Nm$.

B. Experiment 2

The results of the comparison between applying force or torque thresholds is shown by Fig. 8. It can be observed that, as expected, the CS of the robot increased by using $10N$ as thresholds for the contact force in comparison to experiment 1 (cf. Fig. 7). The CS using collision detection based on the torque thresholds listed in IV-C.2 suggests reliable collision detection and identification also at very low robot velocities. Besides at $1.15kg$ and $0.2m/s$ the application of torque thresholds triggered a collision reaction at more sensitive settings than the force threshold. For most sensitive robot performance with the Panda robot, therefore, joint torque thresholds should be applied. Using the colored regions of the CSMs allows to determine in which case a robot integrator needs to make use of torque thresholds and in which cases either contact detection method is suitable. Thus, for robot integration to sensitive tasks the CSMs offer vital information on the required contact detection method.

C. Experiment 3

Fig. 9 depicts the CSMs for the N_4, C_4, and S_4 position for the torque thresholds also used in IV-C.2. The CS appears to be highest at the N_4 position, while the C_4 and S_4 position achieve comparable sensitivity. Based on Fig. 6 we estimated little change between the contact configurations. The CSM supports this hypothesis but shows, nevertheless, that changes in CS occur due to the robot pose at the contact point.Therefore, maps for multiple robot poses need to be obtained to learn about the distribution of the CS within the workspace. This allows defining robot configurations that are most suitable for conducting sensitive tasks.

The experiments demonstrate that CSMs are a useful tool to describe how CS is influenced and that they are, therefore, suited for benchmarking robots or contact detection schemes. Since CS is especially important in collision scenarios, CSMs also enable the planning of a safe HRI. In these experiments, we used a pendulum device to model unconstrained collisions. To investigate CS also in quasi-static contact scenarios, the pendulum load can be increased to obtain high effective masses. In this contact scenario, we expect perfect contact detection for any collaborative robot. In addition, in this study, we focused on obstacle masses for unconstrained collisions related to human body parts. Weights smaller than $1.15kg$ might be of interest f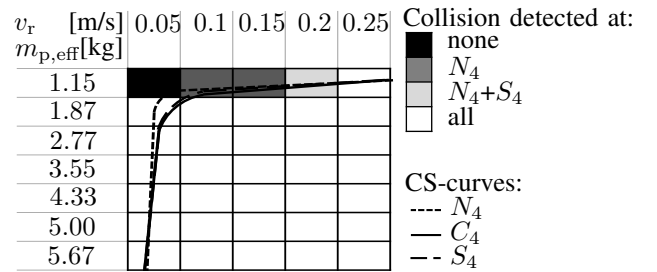or tactile robot applications and should be considered in further studies. Following Fig. 2, we examined object masses and robot velocities that describe the thresholds at which a robot can detect contact. This analysis is based on the assumption that contact detection of all robots does not vary as a function of runtime or system temperature. In further studies, we investigate the repeatability of force/torque detection and collision detection of robots.

VI. CONCLUSION

In this paper, we proposed the concept of a contact sensitivity map (CSM), a novel and convenient tool that allows the robot user to determine whether his/her robot is capable to reliably detect and react to collisions over a range of dynamic collision parameters (mass, velocity) and robot workspace areas. We proposed a standardized benchmark procedure to derive CSMs and provided an implementation based on a pendulum set up. The benchmark experiments were carried out for three robots, namely the Universal Robot's UR10e, UR5e, and Franka Emika Panda. In the experiments, we analyzed the influence of the collision detection method, force/torque thresholds, and the robot configuration. In our results we observe significant differences in terms of CS among the considered robots, collision detection methods and robot poses at contact. Future work will consider testing and comparing further robots and measuring also the force at the contact location to verify the collision detection thresholds. Overall, we believe that the contact sensitivity test should be a standard benchmark test for collaborative robots, as it provides an important assessment of the robot's safety performance.

REFERENCES

[1] ISO/TS 15066. Robots and robotic devices – Collaborative robots. Standard, International Organization for Standardization, Geneva, CH, Feb. 2016.

[2] B. Vemula, B. Matthias, and A. Ahmad. A design metric for safety assessment of industrial robot design suitable for power- and force-limited collaborative operation. *International Journal of Intelligent Robotics and Applications*, 2(2):226–234, 2018.

[3] S. Haddadin, S. Haddadin, A. Khoury, T. Rokahr, S. Parusel, R. Burgkart, A. Bicchi, and A. Albu-Schäffer. On Making Robots Understand Safety: Embedding Injury Knowledge into Control. *International Journal of Robotics Research*, 31:1578–1602, 2012.

[4] N. Mansfeld, M. Hamad, M. Becker, A. G. Marin, and S. Haddadin. Safety map: A unified representation for biomechanics impact data and robot instantaneous dynamic properties. *IEEE Robotics and Automation Letters*, 3(3):1880–1887, Jul. 2018.

[5] A. Schlotzhauer, L. Kaiser, J. Wachter, M. Brandstötter, and M. Hofbaur. On the trustability of the safety measures of collaborative robots: 2d collision-force-map of a sensitive manipulator for safe HRC. In *2019 IEEE 15th International Conference on Automation Science and Engineering (CASE)*, pages 1676–1683, 2019.

[6] S. Haddadin, A. De Luca, and A. Albu-Schäffer. Robot collisions: A survey on detection, isolation, and identification. *IEEE Transactions on Robotics*, 33(6):1292–1312, Dec. 2017.

[7] A. de Luca and R. Mattone. Sensorless robot collision detection and hybrid force/motion control. In *Proceedings of the 2005 IEEE International Conference on Robotics and Automation*, pages 999–1004, 2005.

[8] T. Murakami, F. Yu, and K. Ohnishi. Torque sensorless control in multidegree-of-freedom manipulator. *IEEE Transactions on Industrial Electronics*, 40(2):259–265, 1993.

[9] E. Magrini, F. Flacco, and A. De Luca. Control of generalized contact motion and force in physical human-robot interaction. In *2015 IEEE International Conference on Robotics and Automation (ICRA)*, pages 2298–2304, 2015.

[10] C. D. Santina, R. L. Truby, and D. Rus. Datadriven disturbance observers for estimating external forces on soft robots. *IEEE Robotics and Automation Letters*, 5(4):5717–5724, 2020.

[11] M. Lippi and A. Marino. Enabling physical human-robot collaboration through contact classification and reaction. In *2020 29th IEEE International Conference on Robot and Human Interactive Communication (RO-MAN)*, pages 1196–1203, 2020.

[12] C. P. Neuman and J. J. Murray. Linearization and sensitivity functions of dynamic robot models. *IEEE Transactions on Systems, Man, and Cybernetics*, SMC-14(6):805–818, 1984.

[13] M. Reggiani, M. Mazzoli, and S. Caselli. An experimental evaluation of collision detection packages for robot motion planning. In *IEEE/RSJ International Conference on Intelligent Robots and Systems*, volume 3, pages 2329–2334 vol.3, 2002.

[14] R.J.Kirschner, N. Mansfeld, S. Abdolshah, and S. Haddadin. Experimental analysis of impact forces in constrained collisions according to iso/ts 15066. In *2021 IEEE/ISR International Conference on Intelligence and Safety in Robotics (ISR)*, 2021.

[15] B. Cohen, I. A. Şucan, and S. Chitta. A generic infrastructure for benchmarking motion planners. In *2012 IEEE/RSJ International Conference on Intelligent Robots and Systems*, pages 589–595, 2012.

[16] A. Steinfeld, T. Fong, D. Kaber, M. Lewis, J. Scholtz, A. Schultz, and M. Goodrich. Common metrics for human-robot interaction. In *Proceedings of the 1st ACM SIGCHI/SIGART conference on Human-robot interaction*, pages 33–40, 2006.

[17] ISO 9283:1998-04. Manipulating industrial robots – Performance criteria and related test methods. Standard, International Organization for Standardization, Geneva, CH, April 1998.

[18] ISO/DIS 10218-2:2020(E). Robotics safety requirements for robot systems in an industrial environment part 2: Robot systems, robot applications and robot cells integration. Standard, International Organization for Standardization, Geneva, CH, 2020.

[19] O. Khatib. Inertial properties in robotic manipulation: an object-level framework. *Int. Journal of Robotics Research*, 14(1):19–36, 1995.

[20] C. Gaz, M. Cognetti, A. Oliva, P. Robuffo Giordano, and A. De Luca. Dynamic identification of the franka emika panda robot with retrieval of feasible parameters using penalty-based optimization. *IEEE Robotics and Automation Letters*, 4(4):4147–4154, 2019.